Journal of Cellular Physiology

Bone Marrow Stromal Cells Stimulate an Angiogenic Program that Requires Endothelial MT1-MMP

SURAJ KACHGAL,[1,2] BITA CARRION,[2] ISAAC A. JANSON,[3] AND ANDREW J. PUTNAM[1,2]*

[1]*Department of Biomedical Engineering, University of California, Irvine, Irvine, California*

[2]*Department of Biomedical Engineering, University of Michigan, Ann Arbor, Michigan*

[3]*Department of Materials Science and Engineering, University of Michigan, Ann Arbor, Michigan*

Bone marrow-derived stromal/stem cells (BMSCs) have recently been characterized as mediators of tissue regeneration after injury. In addition to preventing fibrosis at the wound site, BMSCs elicit an angiogenic response within the fibrin matrix. The mechanistic interactions between BMSCs and invading endothelial cells (ECs) during this process are not fully understood. Using a three-dimensional, fibrin-based angiogenesis model, we sought to investigate the proteolytic mechanisms by which BMSCs promote vessel morphogenesis. We find that BMSC-mediated vessel formation depends on the proteolytic ability of membrane type 1-matrix metalloproteinase (MT1-MMP). Knockdown of the protease results in a small network of vessels with enlarged lumens. Contrastingly, vessel morphogenesis is unaffected by the knockdown of MMP-2 and MMP-9. Furthermore, we find that BMSC-mediated vessel morphogenesis in vivo follows mechanisms similar to what we observe in vitro. Subcutaneous, cellular fibrin implants in C.B-17/SCID mice form aberrant vasculature when MMPs are inhibited with a broad-spectrum chemical inhibitor, and a very minimal amount of vessels when MT1-MMP proteolytic activity is interrupted in ECs. Other studies have debated the necessity of MT1-MMP in the context of vessel invasion in fibrin, but this study clearly demonstrates its requirement in BMSC-mediated angiogenesis.

J. Cell. Physiol. 227: 3546–3555, 2012.

The success of engineering viable, functional tissues is contingent on the ability to vascularize the implantable tissue. Limited diffusion of oxygen and other nutrients within tissues greater than 1 cm diminishes the efficacy of simple, specialized tissue implants, thereby necessitating the need to establish penetrating vascular networks within these tissues (Carmeliet and Jain, 2000; Zandonella, 2003). In vivo hypoxic conditions typically result in cells of a mesenchymal lineage mobilizing endothelial cells (ECs) to degrade and invade ischemic tissue through specific proteolytic pathways (Fuchs et al., 2001; Rehman et al., 2004). Understanding the mechanisms that govern this intricate process will be beneficial for the field of regenerative medicine and treating pathologies characterized by aberrant vascularization.

Angiogenesis is vascularization that evolves from new blood vessels sprouting from a parent vessel. Proteases are intimately involved in every phase of angiogenesis starting with the initial degradation of the parent vessel's basement membrane to the final pruning of excess vasculature (Ghajar et al., 2008b). The extracellular matrix (ECM) provides several mechanical and biochemical cues that influence the angiogenic process, including the presentation of protease-cleavable sites that allow interstitial cells and ECs to remodel the ECM. Protease expression, localization, and activation are tightly regulated throughout angiogenesis in a manner that results in focused ECM degradation at the invading vessel front (Kroon et al., 1999; Yana et al., 2007). Matrices that are unable to be remodeled by ECs prevent vessel formation and require the integration of protease-sensitive peptides to accommodate vascularization (Moon et al., 2010; Phelps et al., 2010). The sequence of these peptides should be catered to the protease expression profile of the cells within the implant model. Our group has previously demonstrated that different interstitial cells elicit ECs to use different proteases during angiogenesis (Ghajar et al., 2010; Kachgal and Putnam, 2011); therefore, the choice of interstitial cells is an important factor to consider in designing vascular constructs.

Bone marrow-derived stromal/stem cells (BMSCs) are a type of mesenchymal stem cell that have been extensively characterized in terms of their multipotency (Hauner et al., 1987; Grigoriadis et al., 1988; Ferrari et al., 1998). In addition to their ability to differentiate into a range of tissues, we, along with others, have shown that BMSCs are also capable of promoting angiogenesis (Ghajar et al., 2006; Au et al., 2008; Ghajar et al., 2008a; Ghajar et al., 2010), thereby making them an ideal cell type in engineering specialized, vascularized tissue. BMSCs promote angiogenesis via matrix metalloproteinase (MMP) degradation of the ECM. When cocultured with BMSCs, endothelial MMP-2, MMP-9, and membrane-type 1 (MT1)-MMP upregulation is concomitant with vessel invasion. Additionally, pharmacological inhibition of MMPs completely eliminates BMSC-mediated vessel formation (Ghajar et al., 2010).

The present study explores the specific protease dependency in BMSC-mediated angiogenesis in fibrin. Using RNA interference and an established angiogenesis coculture model (Nakatsu and Hughes, 2008), we show that MT1-MMP is required for BMSC-mediated angiogenesis, whereas the soluble proteases, MMP-2 and MMP-9, are not. Furthermore, MT1-MMP localizes to endothelial tip cells of invading vessels.

Contract grant sponsor: National Institutes of Health;
Contract grant number: R01 HL085339.

*Correspondence to: Andrew J. Putnam, Department of Biomedical Engineering, University of Michigan, 2154 Lurie Biomedical Engineering, 1101 Beal Avenue, Ann Arbor, MI 48109-2110. E-mail: putnam@umich.edu

Manuscript Received: 14 November 2011
Manuscript Accepted: 10 January 2012

Accepted manuscript online in Wiley Online Library (wileyonlinelibrary.com): 19 January 2012.
DOI: 10.1002/jcp.24056

Knockdown of EC MT1-MMP results in the formation of a minimal amount of large, abnormal vessels. Similar abnormal vasculature is found when MMPs are inhibited within BMSC/EC in vivo implants. We also find that EC proliferation is affected by MT1-MMP independent of its catalytic activity. By isolating its proliferation capacity from its proteolytic ability, we find that the catalytic activity of MT1-MMP is, in fact, required for endothelial vessel invasion. These data specifically demonstrate that EC MT1-MMP is absolutely required for BMSC-mediated angiogenesis in fibrin.

Materials and Methods

HUVEC isolation and cell culture

Human umbilical vein endothelial cells (HUVECs) were isolated from freshly harvested umbilical cords as previously described (Ghajar et al., 2006). Briefly, the vein was flushed with sterile phosphate buffered saline (PBS) and then incubated with 0.1% collagenase type I (Worthington Biochemical, Lakewood, NJ) for 20 min at 37°C. The digestion product and subsequent PBS wash were collected and centrifuged. The cell pellet was resuspended in EGM-2 (Lonza, Walkersville, MD), plated onto T-25 flasks, and allowed to attach overnight. PBS was used to wash away any red blood cells the following day. Human BMSCs (Lonza) were cultured in low glucose (1 g/L) DMEM supplemented with 10% fetal bovine serum (FBS, Invitrogen, Carlsbad, CA) and 1% antibiotic-antimycotic (Mediatech, Manassas, VA). Normal human lung fibroblasts (NHLFs, Lonza) were cultured in Medium 199 (Invitrogen) supplemented with 10% FBS and 1% antibiotic–antimycotic. All cultures were incubated at 37°C and 5% CO_2. Media were changed every 2–3 days and cells were harvested with 0.05% trypsin–EDTA (Invitrogen). HUVECs were used prior to passage six, while BMSCs and NHLFs were used prior to passage ten.

Fluorescent labeling of cells

To facilitate visualization and quantification of vessel networks, HUVECs were stably transduced with a gene encoding the mCherry fluorescent protein using the Phoenix Ampho Retrovirus Expression System (Orbigen, San Diego, CA). Phoenix Ampho cells were transfected with a pBMN-mCherry plasmid using Lipofectamine 2000 (Invitrogen). Retroviral supernatant was collected, passed through a 0.45 μm syringe filter, and supplemented with 5 μg/ml Polybrene (Millipore, Billerica, MA) before being incubated with HUVECs for a period of 8 h. This process was repeated the following day. NHLFs were transduced with a GFP adenovirus by adding an adenoviral stock to the culture media for a period of 2 days.

RNA interference

MMP-2 and MMP-9 gene expression levels were attenuated by transducing HUVECs with the HuSH-29 shRNA (OriGene Technologies, Rockville, MD) specific for those two genes. Short-hairpin RNA plasmids for MMP-2 (5′-TATTACCTGAAGCTG-GAGAACCAAAGTCT-3′), MMP-9 (5′-GCCTGCAACGTGAA-CATCTTCGACGCCAT-3′), and a non-targeting control (5′-GCACTACCAGAGCTAACTCAGATAGTACT-3′) were separately packaged into the Phoenix Ampho Retrovirus System (Orbigen) in a similar fashion as the aforementioned mCherry plasmid. HUVECs were incubated with the filtered retroviral supernatant for a period of 10 h each day for four consecutive days. A lentiviral shRNA plasmid against MT1-MMP (5′-GCGATGAA-GTCTTCACTTACTTCT-3′) and a corresponding scrambled shRNA (5′-CAACAAGATGAAGAGCACCAA-3′) plasmid were graciously provided by Dr. Mina J. Bissell. These plasmids were packaged into lentiviral particles using the Virapower Lentiviral Expression System (Invitrogen). The lentiviral shRNA plasmids, along with the packaging plasmids, were transfected into 293FT cells using Lipofectamine 2000. After a 48-h incubation period, the lentiviral supernatant was collected and passed through a 0.45-μm syringe filter. The supernatant was concentrated by ultracentrifugation at 77,000*g* for 90 min, followed by resuspension in PBS. HUVECs were incubated in EGM-2 supplemented with 5 μg/ml Polybrene for 30 min at 37°C prior to the addition of the concentrated lentiviral supernatant. The lentiviral medium was removed after 48 h and replaced with fresh EGM-2. Selection of shRNA-expressing HUVECs was achieved by culturing HUVECs in the presence of 1 μg/ml puromycin (Sigma-Aldrich, St. Louis, MO) for a period of 4–6 days. MT1-MMP knockdown in BMSCs was carried out via electroporation. Small-interfering RNAs against MT1-MMP (5′-AACAGGCAAAGCTGAT GCAGA-3′) and a scrambled control (5′-AAGTGATCAAGCACCGAAGAG-3′) were graciously provided by Dr. Stephen J. Weiss. Each respective siRNA was introduced into BMSCs at a concentration of 40 nM using the Nucleofector Kit for Human Mesenchymal Stem Cells and Nucleofector Device (Lonza).

MT1-MMP constructs

Plasmids encoding for MT1-MMP constructs with a deleted catalytic domain (ΔCAT-MT1) and the full-length form (Full-MT1) were previously characterized (Mori et al., 2009) and graciously donated by Dr. Mina J. Bissell and Dr. Stephen J. Weiss, respectively. In addition, a fluorescently-tagged MT1-MMP construct was created by EGFP fusion onto the C-terminus of the full length form. These constructs were subsequently cloned into the pBMN retroviral vector. Retroviral particles were created using the aforementioned Phoenix Ampho Expression system and HUVECs were transduced with the retroviral supernatant for a period of 10 h for two consecutive days.

Reverse transcription and quantitative polymerase chain reaction

Total RNA was isolated from cells using the SV Total RNA Isolation System (Promega, Madison, WI) and quantified using a Nanodrop ND-1000 (Thermo Fisher Scientific, Rochester, NY). Equal amounts of total RNA from each sample in its respective experimental group were used to create first-strand cDNA using the ImProm-II Reverse Transcription System (Promega). Quantitative PCR (qPCR) was performed using a 7500 Fast Real-Time PCR System and TaqMan Universal PCR Master Mix (Applied Biosystems, Carlsbad, CA). Predesigned qPCR primers for human MMP-2, MMP-9, MT1-MMP, and 18s rRNA were selected from the TaqMan Gene Expression Assays database (Applied Biosystems). The $\Delta\Delta C_T$ method was used to assess the relative quantity of each target gene.

Fibrin tissue assembly

Cytodex 3 microcarrier beads (Sigma-Aldrich) were subjected to a series of washes in EGM-2, and then added to a HUVEC suspension in a 5-ml polypropylene tube at a ratio of 400 cells/bead. To promote cell coating onto the beads, the suspension was mixed by gentle pipetting every 30 min for 3.5 h. Afterwards, the bead solution was collected and transferred into an upright T-25 flask with an additional 1.5 ml EGM-2. This flask was cultured overnight at 37°C and 5% CO_2 to allow any remaining suspended cells to attach to the culture surface. The following day, fibrinogen (Sigma-Aldrich) was dissolved in serum-free EGM-2 to a final concentration of 2.5 mg/ml. The solution was passed through a 0.22 μm syringe filter before being combined with the appropriate interstitial cell type (100,000 cells/ml) and HUVEC-coated beads (50 beads/ml). For each gel to be constructed, 10 μl of a 50 U/ml thrombin solution (Sigma-Aldrich) was added to the center of a well of a 24-well tissue culture plate. Immediately prior to polymerization, 5% FBS was added to the fibrinogen solution followed by addition of 500 μl to each of the thrombin-spotted wells. The solution was initially allowed to set for 5 min at room

temperature followed by incubation at 37°C and 5% CO_2 for an additional 30 min. Following polymerization, fully-supplemented EGM-2 and any chemical inhibitors were added. Medium (± chemical inhibitors) was changed at day 1, 3, and 5 post-assembly. For the purposes of high-magnification imaging, tissue constructs were also formed in 8-well chambered coverglass with number 1 thickness.

Fluorescence imaging and quantification

Fluorescent images were captured using an Olympus IX81 equipped with a Disc Scanning Unit and a 100 W high-pressure mercury burner (Olympus America, Center Valley, PA), a Hamamatsu Orca II CCD camera (Hamamatsu Photonics, K.K., Hamamatsu City, Japan), and Metamorph Premier software (Molecular Devices, Sunnyvale, CA). Total vessel network formation was assessed 7 days post-assembly. Imaged beads were chosen at random provided that they met the condition that vessels emanating from a given bead did not form anastomoses with vessels from adjacent beads. At least five beads per condition were imaged at low magnification (4×) for each independent experiment. Total vessel network length was measured utilizing the Angiogenesis Tube Formation module in Metamorph. Minimum and maximum widths were entered into the program to differentiate vessels from noise and the bead, respectively. Cell proliferation was assessed by capturing four non-overlapping, low magnification (4×) images per condition of HUVECs stained with 200 ng/ml 4′,6-diamidino-2-phenylindol (DAPI, Sigma-Aldrich). The total number of cells were counted using the Count Nuclei module in Metamorph and then normalized to the first time point assessed.

In vivo vascularization and histology

Animal procedures were performed in accordance with the National Institutes of Health's guidelines for laboratory animal usage following a protocol approved by the University of Michigan University Committee on Use and Care of Animals. Tissue constructs were prepared for injection by combining 1.5 million HUVECs and 1.5 million BMSCs in 300 μl of a 10 mg/ml fibrinogen/EGM-2 (minus FBS) solution. C.B-17/SCID male mice (Taconic, Hudson, NY) aged 4 weeks were used for all experiments. A prepared anesthetic/analgesic cocktail of ketamine (100 mg/kg), xylazine (10 mg/kg), and buprenorphine (0.05 mg/kg) (Western Medical Supply, Arcadia, CA) was delivered via an intraperitoneal injection. The dorsal area of each animal was subsequently shaved and sterilized with betadine (Thermo Fisher Scientific). Immediately prior to implant injection, 15 μL FBS, 6 μl of a 50 U/ml thrombin solution, and any chemical inhibitors were added to the precursor solution. The gel precursor solutions were injected subcutaneously into the rear, lateral flanks so that each mouse carried two implants. The mice were kept stationary for 5 min to aid in the initial polymerization of the gel solution and then transferred to their recovery cages. Mice were sacrificed at 7 days post-implantation and implants were retrieved and immediately placed in 10% formalin (Sigma-Aldrich). The implants were transferred into PBS the following day and stored at 4°C. Samples were forwarded to AML Laboratories (Baltimore, MD) for histological sectioning and hematoxylin and eosin (H&E) staining. Quantification of perfused vessels was assessed independently by two individuals who were blinded to the study and sample conditions. Each individual was asked to count the number of vessels filled with erythrocytes within several 40× H&E-stained images.

Other reagents used

The broad spectrum MMP inhibitor GM6001 (EMD Chemicals, Gibbstown, NJ) was used at a greater than 100-fold excess (10 μM) of its IC50 concentrations against MMP-2, MMP-9, and MT1-MMP (Uttamchandani et al., 2007). To minimize evaluating the off-target effects that individual pharmacological inhibitors may cause, the more potent MMP inhibitor BB2516 (Tocris Bioscience, Ellisville, MO) was used at 3.3 μM, which represents a comparable level of inhibition to 10 μM GM6001, based on the supplier's IC50 values for the same MMPs. Additionally, 100 μM of GM6001 was added to the fibrinogen gel precursor solutions to inhibit MMP activity in vivo. Equal volumes of dimethyl sulfoxide (DMSO, Sigma-Aldrich) were used as the vehicle control for these experiments.

Statistical analysis

Statistical analyses were performed using GraphPad Prism software (GraphPad Software, La Jolla, CA). Data are presented as mean ± standard deviation. One-way analysis of variance with a Bonferroni post test was used to assess statistical significance between data sets. Statistical significance was assumed when $P \leq 0.05$.

Results

BMSC-mediated angiogenesis in fibrin is not dependent on soluble MMPs

To systematically assess the requirement of specific proteases in BMSC-mediated angiogenesis, we first used retroviral shRNAs against the soluble MMPs, MMP-2 and MMP-9, to attenuate their expression in HUVECs, and then cocultured these cells with BMSCs in our angiogenesis model. Knockdown of MMP-2 expression, as measured through qPCR, was found to be 76% relative to the non-targeting shRNA (shNT, Fig. 1A). Expression of MMP-9 was not detected in either shNT or shMMP-9 HUVECs. This is consistent with our previous RT-PCR findings that MMP-9 expression in HUVECs was seen only when cocultured with BMSCs and not when cultured alone (as they were when RNA lysates were obtained for qPCR) (Ghajar et al., 2010). Regardless, neither shMMP-2 nor shMMP-9 HUVECs displayed any difference in vessel sprouting with respect to shNT HUVECs (Fig. 1B,C). A pan-specific MMP inhibitor, BB2516, was used as a control that drastically inhibits vessel sprouting in BMSC/HUVEC cocultures.

MT1-MMP expression in HUVECs is required for BMSC-mediated angiogenesis in fibrin

Previous studies from our group and others have shown a positive correlation between vessel sprouting and MT1-MMP expression (Hotary et al., 2002; Ghajar et al., 2006, 2010; Yana et al., 2007). Knockdown of HUVEC MT1-MMP expression via lentiviral shRNA was assessed to be 72% relative to the scrambled shRNA (shSCR, Fig. 2A). HUVECs transduced with the shMT1 lentivirus demonstrated a 72% reduction in total vessel network sprouting relative to the shSCR HUVECs when both were cocultured with BMSCs (Fig. 2B,C). The minimal vessels that did sprout in the shMT1 HUVEC condition displayed a qualitatively thickened morphology (Fig. 2C arrowheads). This abnormal vessel morphology is phenotypically similar to what we have observed when using the pan-specific MMP inhibitor GM6001 in adipose-derived stem cell/HUVEC (Kachgal and Putnam, 2011) and fibroblast/HUVEC cocultures (Fig. 3A). In these cultures, total vessel network length is not affected by MMP-inhibition, but the formed vessels are thicker than their respective controls. Fibroblast/HUVEC cocultures also showed altered, and seemingly insufficient, pericytic coverage of vessels when MMPs were inhibited (Fig. 3B).

MT1-MMP has previously been shown to localize to the tip of invading vessels in collagen gels, thereby imparting a polarity between endothelial tip cells and vessel stalk cells (Yana et al., 2007). We created an MT1-MMP-GFP fusion construct so as to visualize the localization of MT1-MMP in sprouting vessels. HUVECs were transduced with the retroviral MT1-MMP-GFP construct and cocultured with BMSCs within our angiogenesis

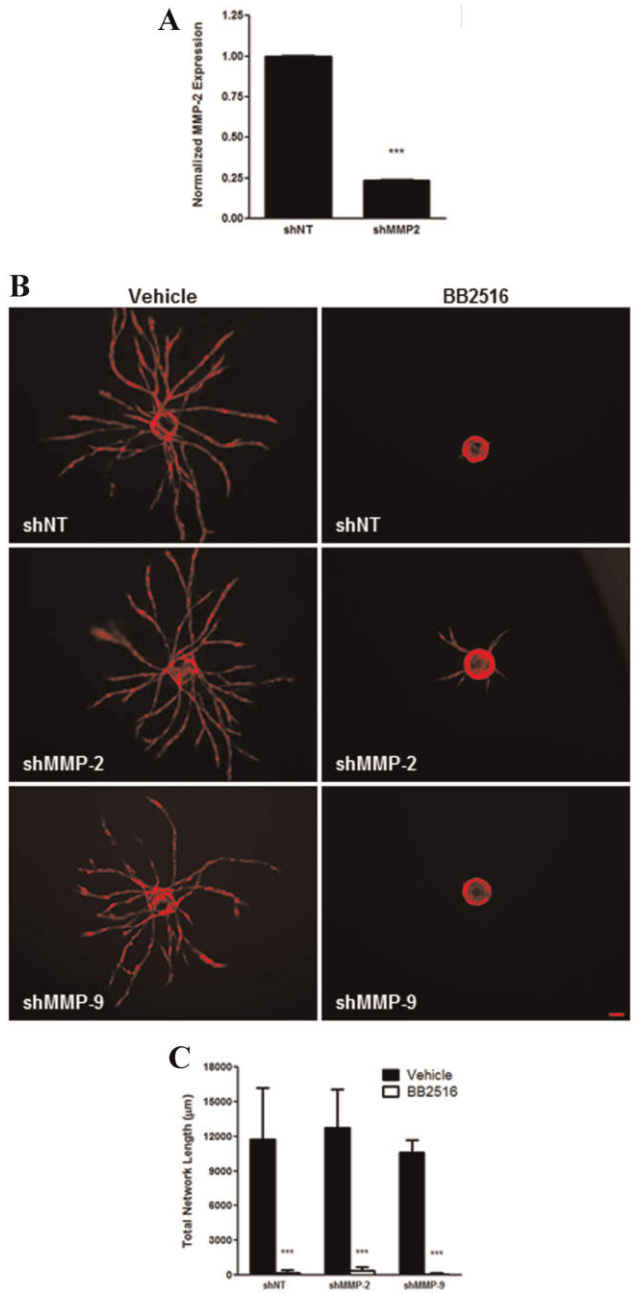

Fig. 1. BMSC-mediated angiogenesis is not mediated by MMP-2 and MMP-9. HUVECs, transduced with mCherry and either an shRNA against MMP-2, MMP-9, or a non-targeting (NT) control, were coated on microcarrier beads and cultured within 2.5 mg/ml fibrin gels interspersed with BMSCs. A: Expression level of MMP-2 in HUVECs after knockdown was assessed via qPCR. MMP-9 expression was not detected in either shNT or shMMP-9 HUVECs. B: Representative day 7 images of vessel formation in the presence of either a DMSO vehicle control (left column) or 3.3 μM of MMP-inhibitor, BB2516 (right column). C: Quantification of total vessel network length at day 7. * refers to $P \leq 0.001$ in comparison to the respective controls. Scale bar = 100 μm. [Color figure can be seen in the online version of this article, available at http://wileyonlinelibrary.com/journal/jcp]**

model. At day 3, MT1-MMP localized to the tips of nascent vessels (Fig. 4 top panel arrow). High-magnification imaging of the endothelial vessel tips reveals further MT1-MMP expression within the filopodia extending from the vessel tip (Fig. 4 bottom panel arrowheads).

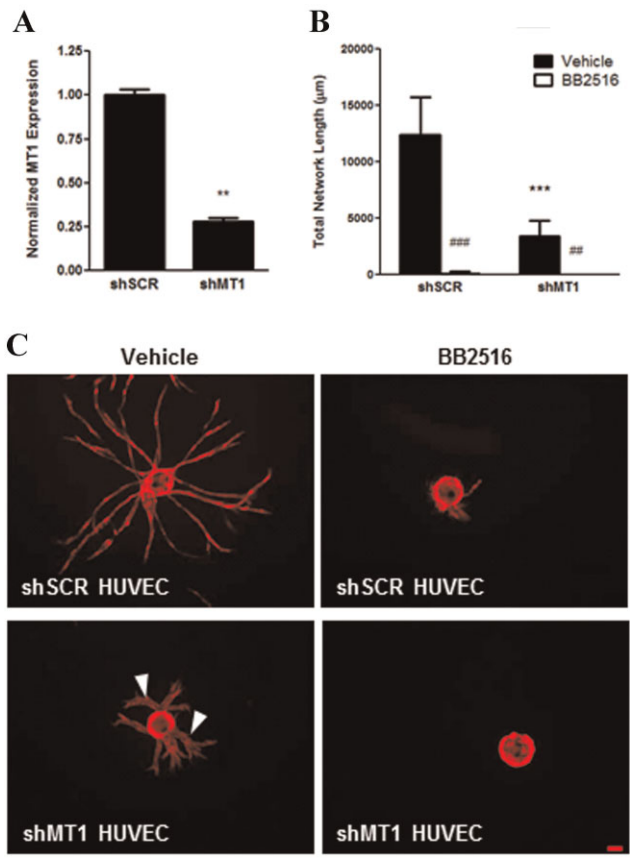

Fig. 2. Knockdown of MT1-MMP in HUVECs diminishes vessel sprouting and effects vessel diameter. A: Expression level of MT1-MMP in HUVECS after knockdown as assessed via qPCR. B: Quantification of total vessel network length at day 7. C: day 7 images of mCherry-expressing HUVECs, transduced with either an shRNA against MT1-MMP or a scrambled control (shSCR), on microcarrier beads cocultured with BMSCs within a fibrin matrix either in the presence of a DMSO vehicle control (left panel) or 3.3 μM BB2516 (right panel). Arrowheads indicate thickened vessels as a result of MT1-MMP knockdown. ** in (A) refers to $P \leq 0.01$ with respect to the scrambled control. * in (C) refers to $P \leq 0.001$ with respect to the shSCR vehicle control condition. ## and ### refer to $P \leq 0.01$ and 0.001 in comparison to the vehicle control conditions, respectively. Scale bar = 100 μm. [Color figure can be seen in the online version of this article, available at http://wileyonlinelibrary.com/journal/jcp]**

To determine whether MT1-MMP expression in the interstitial cell compartment is also required for angiogenesis, we introduced an siRNA against MT1-MMP into BMSCs via electroporation. Knockdown, as assayed by qPCR, was shown to be 89% relative to BMSCs electroporated with a scrambled siRNA (siSCR, Fig. 5A). Coculture of siMT1 BMSCs with wild type (WT)-MT1-MMP HUVECs showed no significant difference in vessel sprouting relative to siSCR BMSCs (Fig. 5B,C).

Catalytic activity of MT1-MMP in HUVECs is required for BMSC-mediated angiogenesis in fibrin

Recent studies have postulated non-proteolytic functions for MT1-MMP (Mori et al., 2009; Lu et al., 2010). Therefore, knockdown of MT1-MMP may have an effect on HUVECs outside of its proteolytic capability. Since EC proliferation is also a hallmark of the angiogenic process, especially at the MT1-MMP-rich vessel tip (Yana et al., 2007), we assessed the

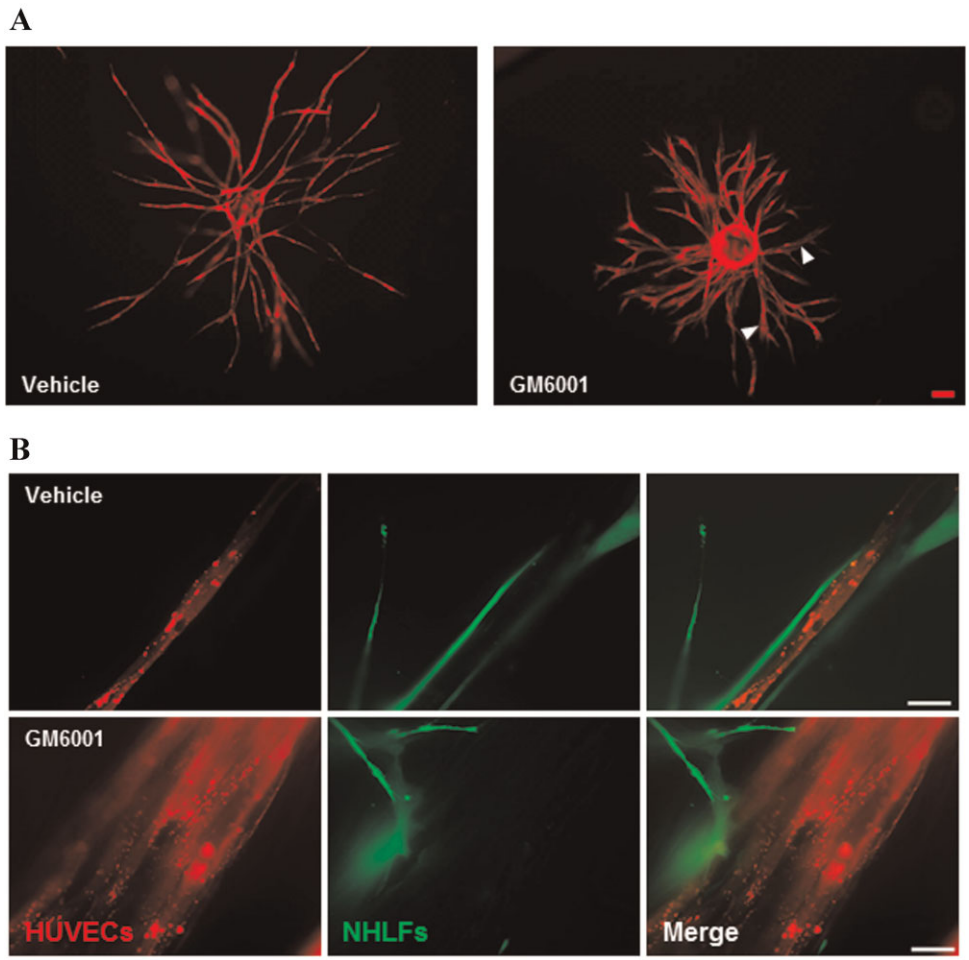

Fig. 3. MMP-inhibition in fibroblast-mediated angiogenesis results in thickening of vessels and altered pericytic coverage of vessels. A: day 7 images of fluorescently-transduced HUVECs on microcarrier beads cocultured with lung fibroblasts within a fibrin matrix either in the presence of a DMSO vehicle control (left panel) or 10 μM of MMP-inhibitor, GM6001 (right panel). Arrowheads indicate thickened vessels as a result of MMP inhibition. B: Fibroblasts (green) were cultured with HUVECs (red) in the presence of DMSO (top row) or GM6001 (bottom row) for 7 days. Pericytic association of fibroblasts with the vessels was assesed via high-magnification confocal microscopy. Scale bar in (A) = 100 μm. Scale bar in (B) = 20 μm. [Color figure can be seen in the online version of this article, available at http://wileyonlinelibrary.com/journal/jcp]

proliferative capacity of shMT1-transduced HUVECs. HUVECs were transduced with two separate lentiviral shRNA clones against MT1-MMP and proliferation was assayed at day 3 by counting DAPI-stained nuclei and normalizing them to their respective day 1 count. The shMT1 clones 348 and 1644 had knockdown efficiencies of 41 and 89%, respectively (Fig. 6A), and significantly decreased HUVEC proliferation by 35 and 44%, respectively (Fig. 6B,C).

In order to delineate the effects of MT1-MMP on BMSC-mediated angiogenesis, we sought to determine whether the lack of sprouting identified in BMSC/shMT1 HUVEC cocultures (Fig. 2B,C) was due to MT1-MMP's proteolytic ability or its effect on EC proliferation. HUVECs were transduced with a retrovirus encoding for either an MT1-MMP mutant lacking the catalytic domain (ΔCAT-MT1) or a control encoding for the full-length construct (Full-MT1, Fig. 6C). Total MT1-MMP expression in Full-MT1 and ΔCAT-MT1 HUVECs was five and 85-fold greater than WT cells, respectively (Fig. 6D). When cocultured with BMSCs, WT, and Full-MT1 HUVECs displayed no significant difference in total vessel network formation; whereas ΔCAT-MT1 HUVECs exhibited a dramatic decrease relative to the former two conditions (Fig. 6E,F). Interestingly, ΔCAT-MT1 vessels did not exhibit the thickened morphology characteristic of those formed from shMT1 HUVECs. The proliferative effects of MT1-MMP on HUVECs were effectively segregated from its proteolytic ability, as both Full-MT1 and ΔCAT-MT1 HUVECs displayed similar proliferation potentials (Fig. 6G).

MMP activity is required to establish normalized vasculature in vivo

To assess the MMP-dependency of vascularization in vivo, we subcutaneously injected a fibrin gel precursor solution containing BMSCs and HUVECs along with the broad-spectrum MMP inhibitor GM6001 or a DMSO vehicle control into C.B-17/SCID mice. H&E staining of retrieved implants at day 7 revealed abnormal vasculature in implants that were dosed with GM6001. The vessels appeared large relative to the vehicle control and tended to coalesce into pockets throughout the implant, characteristic of a hemangioma (Fig. 7A). Implants from both conditions formed anastomoses with the host vasculature as evidenced by the presence of erythrocytes within vessel lumens (Fig. 7A arrows); however, several of the vessels in the

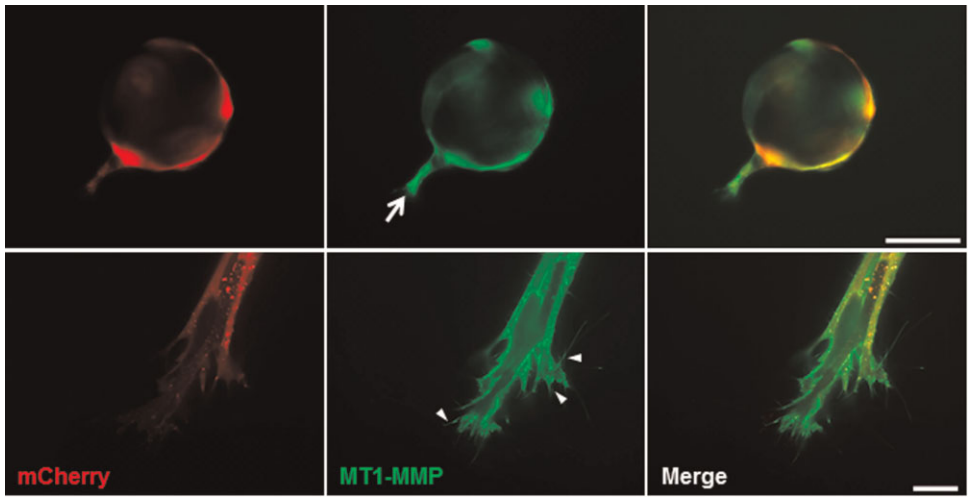

Fig. 4. Endothelial vessel tips strongly express MT1-MMP. HUVECs were transduced with mCherry and an MT1-MMP-GFP construct, coated on microcarrier beads, then cocultured with BMSCs within a fibrin matrix. Day 3 images show strong expression of MT1-MMP in the tip of a budding vessel (top panel, arrow). High-magnification imaging shows further MT1-MMP localization to vessel tips as well as to extending filopodia (bottom panel, arrowheads). Top panel scale bar = 100 μm. Bottom panel scale bar = 20 μm. [Color figure can be seen in the online version of this article, available at http://wileyonlinelibrary.com/journal/jcp]

GM6001 condition exhibited incomplete walls resulting in extravasation of erythrocytes into the interstitial matrix (Fig. 7A arrowheads).

In order to more specifically assess the effects of MT1-MMP in vivo, ΔCAT-MT1 HUVECs and BMSCs were implanted subcutaneously within a fibrin gel. Gross visualization of implants retrieved at day 7 revealed a marked decrease in blood perfusion within the ΔCAT-MT1 HUVEC/BMSC implants as compared to the Full-MT1 HUVEC/BMSC implants (Fig. 7B). Subsequent H&E staining of implant sections validated these findings as Full MT1 HUVEC/BMSC implants displayed an abundant number of perfused vessels whereas ΔCAT-MT1 HUVEC/BMSC implants had significantly less vessel formation (Fig. 7C,D).

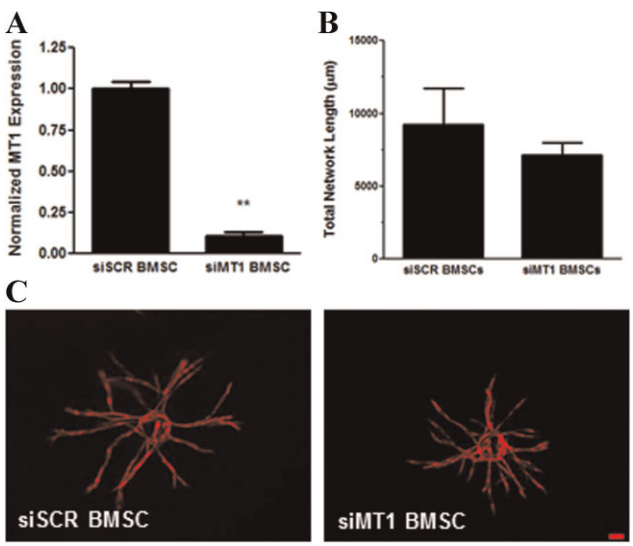

Fig. 5. BMSC-derived MT1-MMP is not required for vessel sprouting. BMSCs were electroporated with siRNA against either MT1-MMP or a scrambled control (siSCR) and then cocultured with mCherry-expressing HUVECs on microcarrier beads. A: BMSC MT1-MMP expression levels as assessed via qPCR. B: Quantification of total vessel network length at day 7. C: Representative day 7 images of vessel formation. ** refers to $P \leq 0.01$ with respect to the scrambled control. Scale bar = 100 μm. [Color figure can be seen in the online version of this article, available at http://wileyonlinelibrary.com/journal/jcp]

Discussion

This study explored the proteolytic mechanisms that guide BMSC-mediated angiogenesis within a fibrin matrix. We have previously found that chemical inhibition of MMPs in BMSC/HUVEC cocultures abrogated vessel formation (Ghajar et al., 2010). Here, we used RNA interference to demonstrate that EC invasion and subsequent normal vessel formation are dependent on the proteolytic activity of MT1-MMP, and do not absolutely require MMP-2 or MMP-9. Knockdown of endothelial MT1-MMP severely limited vessel network formation, but did allow formation of a short network of vessels with abnormally enlarged lumens; this phenotype is similar to that observed when MMPs were inhibited in fibroblast/HUVEC angiogenesis models. Furthermore, these findings were also validated in vivo, as pharmacological inhibition of MMPs resulted in the formation of abnormal vasculature in cellular fibrin implants, and specific deletion of the proteolytic domain of MT1-MMP significantly hindered any vessel formation.

Heterotypic interactions between BMSCs and ECs have been previously shown to influence vessel formation and invasion within fibrin matrices (Ghajar et al., 2010). We, along with other groups, have previously shown that the expression of MMP-2, MMP-9, and MT1-MMP are all upregulated in BMSC/EC cocultures (Hanemaaijer et al., 1993; Brooks et al., 1996; Ghajar et al., 2006; Ghajar et al., 2010), but only the knockdown of the membrane-bound MT1-MMP inhibited vessel invasion. This is consistent with our previous study that found that TIMP-2, but not TIMP-1, abrogated vessel sprouting in BMSC/HUVEC cocultures (Ghajar et al., 2010). These data suggest that vessel invasion requires anchored proteases at the vessel tip, degrading the ECM in a tightly guided fashion, rather than soluble proteases whose activities are likely not as spatially

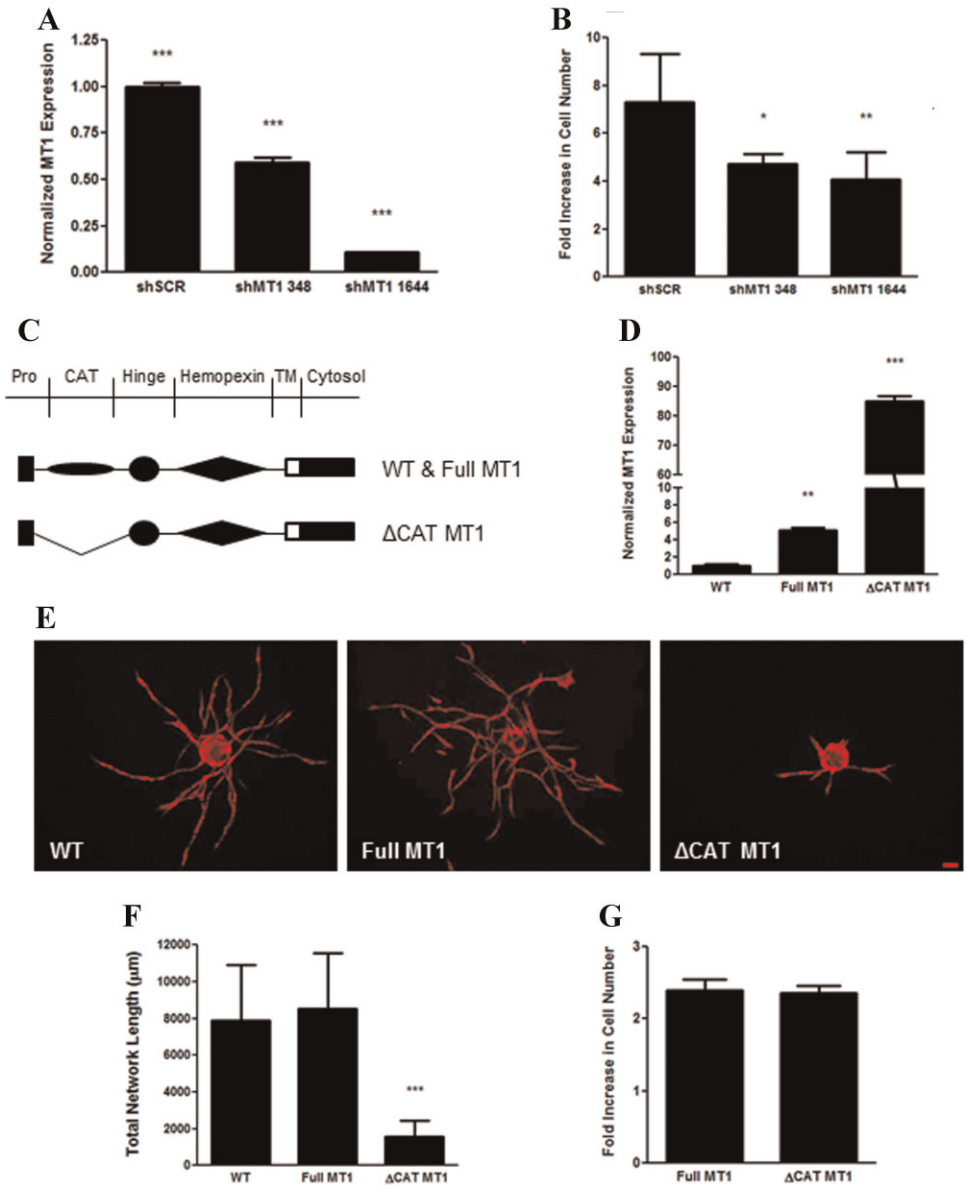

Fig. 6. MT1-MMP knockdown also reduces HUVEC proliferation, but its proteolytic activity is required for angiogenesis. HUVECs were transduced with separate shRNA clones against MT1-MMP or a scrambled control. A: MT1-MMP expression as assessed via qPCR. B: DAPI-stained HUVEC cultures were counted at day 3 and normalized to the count at day 1 to assess proliferation. C: HUVECs were transduced with either an MT1-MMP construct with a deleted catalytic domain (ΔCAT-MT1) or the full-length construct (Full-MT1). D: Total MT1-MMP expression relative to wild type (WT) HUVECs as assessed via qPCR. These HUVECs along with a WT control were transduced with mCherry before being coated on microcarrier beads and cocultured with BMSCs within a fibrin matrix. Representative images (E) and quantification (F) of total vessel network length at day 7. G: Full-MT1 and ΔCAT-MT1 HUVECs were DAPI-stained and counted at day 3 and normalized to the day 1 count to assess proliferation. * in (A) refers to $P \leq 0.001$ for each group in comparison to each other group. * and ** in (B) refer to $P \leq 0.05$ and 0.01 in comparison to the shSCR condition, respectively. ** and *** in (D) refer to $P \leq 0.01$ and 0.001 in comparison to the WT control, respectively. *** in (F) refers to $P \leq 0.001$ with respect to each of the other two groups. Scale bar = 100 μm. [Color figure can be seen in the online version of this article, available at http://wileyonlinelibrary.com/journal/jcp]**

restricted. This theory is consistent with our previous reports that fibroblast and adipose-derived stem cell-mediated angiogenesis can proceed through a urokinase plasminogen activator (uPA)-directed mechanism (Ghajar et al., 2010; Kachgal and Putnam, 2011). Plasminogen activation into the serine protease plasmin occurs through two mechanisms: uPA or tissue plasminogen activator (tPA). The former pathway requires initial binding of uPA to the cell membrane-anchored uPA receptor, thereby sequestering plasmin activation and proteolysis to the immediate vicinity of the cell surface. Conversely, activation by tPA does not require prior binding to a cell surface receptor, and results in a global activation of plasmin. We have observed bulk degradation of fibrin gels without vessel formation in cultures that express excessive tPA (unpublished observations). MMP-2 and MMP-9 have demonstrated the ability to localize to the cell surface through the binding of $\alpha_V\beta_3$ and CD44, respectively; however, the endothelial expression of these molecules within a fibrin matrix is unclear as they are classically known as adhesion molecules for fibronectin and hyaluronic acid, respectively (Brooks et al.,

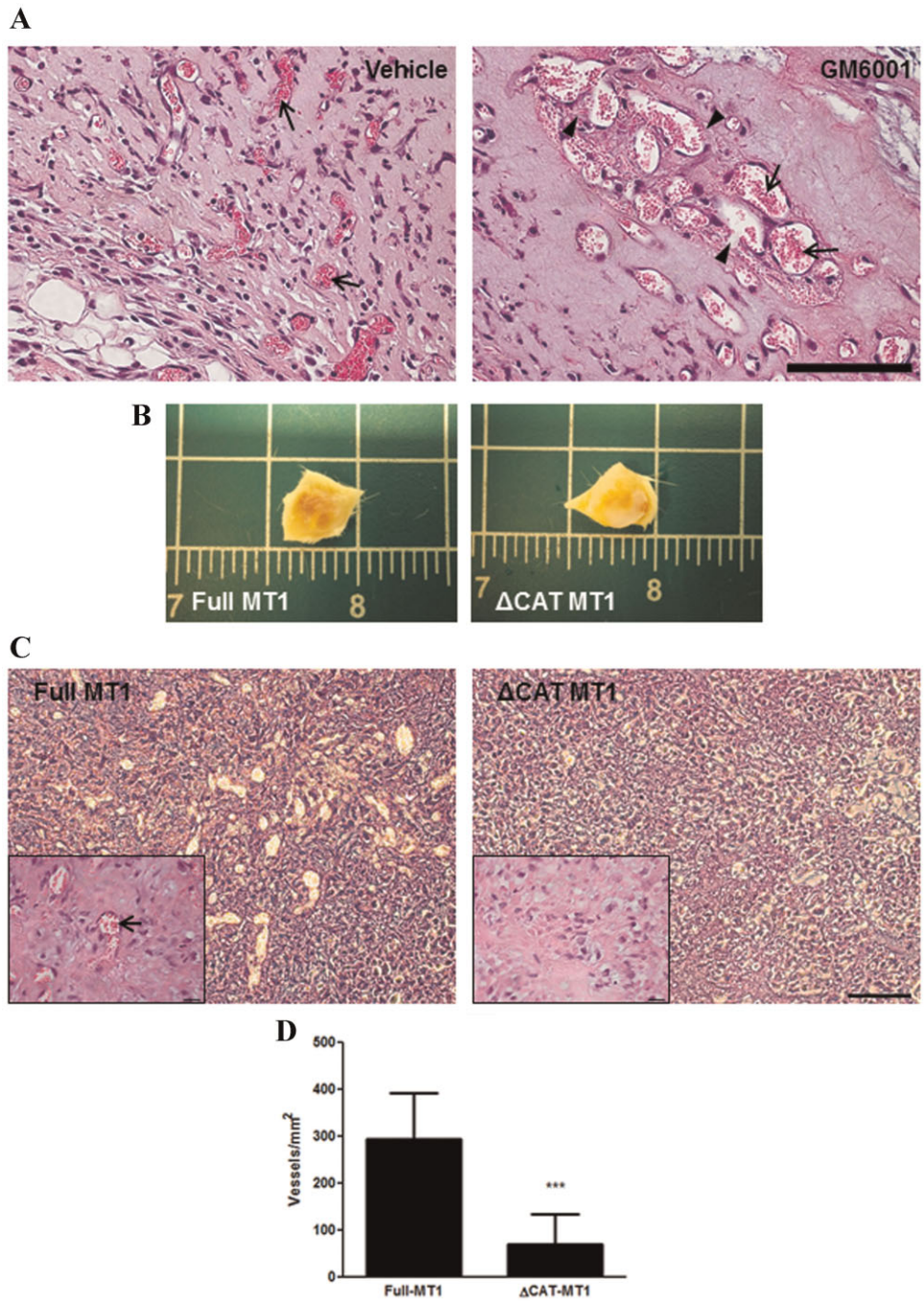

Fig. 7. MMPs are required for establishing normal in vivo vasculature. BMSCs and HUVECs were subcutaneously injected within a fibrin matrix into C.B-17/SCID mice. A: Erythrocytes (arrows), indicative of anastomosis with host vasculature, can be observed in hematoxylin and eosin-stained sections of implants retrieved at day 7. Erythrocyte extravasation from vessels with discontinuous lumenal walls can be observed in implants pre-dosed with GM6001 (arrowheads). B: day 7 retrieval of ΔCAT-MT1 HUVEC/BMSC implants revealed a reduced level of vascularization compared to Full-MT1 HUVEC/BMSC implants. C: H&E-stained sections reveal extensive, perfused vasculature in Full-MT1 HUVEC/BMSC implants and no vascularization of ΔCAT-MT1 HUVEC/BMSC implants. Insets show magnified images of respective sections. Arrow shows erythrocytes within vessel lumen. D: Quantification of perfused vessels per millimeter. Scale bars in (A and C) = 100 μm. Scale in (B) is shown in inches. Scale bar in (C, inset) = 20 μm. [Color figure can be seen in the online version of this article, available at http://wileyonlinelibrary.com/journal/jcp]

1996; Yu and Stamenkovic, 1999). The upregulation of MMP-2 and MMP-9 that we have previously documented could be a consequence of both MMPs being activated by MT1-MMP (Sato et al., 1994; Toth et al., 2003), and play a role in assisting MT1-MMP with ECM degradation, but our data here show that they are nonessential to the overall angiogenic process in a fibrin matrix.

In addition to its effect on outward vessel invasion, MT1-MMP knockdown yielded vessels that exhibited a thicker morphology than their control counterparts. Similarly enlarged

vessels were observed when MMP activity was disrupted with a broad spectrum MMP inhibitor in fibroblast/EC cocultures, correlating with a decrease in fibroblast pericytic coverage of the vessels. This finding of enlarged vessels also translated to the in vivo setting where we showed hemangioma-like vasculature development when MMPs were inhibited. While the contribution of macrophage-derived proteases to tumor angiogenesis has been shown (Hildenbrand et al., 1995; Gocheva et al., 2010a,b), these are unlikely to be a major determinant of vascularization in this scenario; deletion of the catalytic domain of HUVEC MT1-MMP was sufficient to completely inhibit vessel formation. These data suggest that MT1-MMP also exerts an effect on regulating vessel diameter, and perhaps stabilizing neovessels. Perivascular association of mural cells is known to stabilize nascent vasculature and influence vessel distention (Hellstrom et al., 2001; Morikawa et al., 2002). Prior studies have shown that MT1-MMP expression in the mural cell compartment is required for migration and association of mural cells with neovessels (Filippov et al., 2005; Lehti et al., 2005; Sounni et al., 2010); however, knockdown of MT1-MMP in BMSCs did not noticeably affect vessel diameter, suggesting rather that MT1-MMP within the EC compartment is responsible for regulating vessel diameter, at least within fibrin matrices. Another theory for this phenomenon involves the local concentration of vascular endothelial growth factor (VEGF) in the vessel microenvironment. High local concentrations of VEGF have been shown to promote hemangioma formation (Ozawa et al., 2004). With increasing evidence suggesting that MMPs serve an additional role in releasing matrix-bound growth factors (Egeblad and Werb, 2002; Heissig et al., 2003), it is possible that MMP inhibition in ECs prevents the release and internalization of VEGF; this might lead to sustained high local concentrations of VEGF that support a pro-angiogenic phenotype rather than switching to a maturation phenotype.

MT1-MMP had an additional effect on the proliferation of ECs. Knockdown of HUVEC MT1-MMP resulted in an unexpected reduction of their proliferative capacity. ECs at vessel tips had previously been shown to express a higher level of MT1-MMP and be more proliferative than vessel stalk cells (Yana et al., 2007), but these have not been directly linked. Our data showed a strong localization of MT1-MMP to the vessel tips. These data, taken together, opened the possibility that the lack of angiogenesis in MT1-MMP-deficient HUVECs was a consequence of their decreased proliferation rather than limited ECM degradation. To isolate MT1-MMP's effect on proliferation from its effect on ECM degradation, we transduced HUVECs with a truncated form of MT1-MMP lacking its catalytic domain. These cells had similar proliferation potential as HUVECs transduced with full-length MT1-MMP, yet displayed severely inhibited vessel network formation when cocultured with BMSCs. Furthermore, ΔCAT-MT1 HUVECs inhibited vessel formation within fibrin implants in vivo when cocultured with BMSCs. These data clearly demonstrate that MT1-MMP proteolytic activity is required for BMSC-mediated vessel formation in fibrin matrices. Interestingly, ΔCAT-MT1 vessels did not exhibit enlarged lumens as shMT1 vessels did.

Beyond addressing key, underlying mechanisms involved in BMSC-mediated angiogenesis, this work has implications toward the design of biomaterials that support neovascularization. As mentioned earlier, the ability to create vascularized, specialized tissues might alleviate several of the problems associated with ischemia-induced implant necrosis. Our use of a fibrin matrix is predicated on its role as a provisional matrix and site of angiogenesis in natural wound healing (van Hinsbergh et al., 2001). Fibrin is also a natural attractant of mesenchymal cells such as BMSCs (Clark, 2001; Farrell and al-Mondhiry, 1997), which are thought to remain quiescent until activated by tissue injury (Caplan, 2008; Crisan et al., 2008), whereby they promote tissue regeneration instead of fibrosis. Additionally, BMSCs are thought to differentiate toward the lineage of the injured tissue to further support tissue regeneration. However, the clinical use of fibrin as a biomaterial has some potential limitations. Chief among these is the sourcing of the precursor fibrinogen. Traditional fibrin-based surgical adhesives source their fibrinogen, and associated clotting factors, from pooled human plasma fractions, which can incur the risk of viral transmission (Siedentop et al., 1985). Obtaining fibrinogen from autologous sources greatly reduces this risk, but is not always practical due to time constraints. Another concern is bulk proteolysis of the fibrin by host proteases following implantation. Current strategies require the co-delivery of fibrinolytic inhibitors to prevent premature ECM degradation (Webster and West, 2002), but for the purposes of our vascular constructs, these inhibitors may prevent matrix remodeling and vascularization altogether.

Recent efforts have been made to promote vessel formation within synthetic matrices, which would potentially negate the issues associated with natural material sourcing (Moon et al., 2010; Phelps et al., 2010). In many cases, the degradability of synthetic materials can be tuned via the inclusion of protease-cleavable peptide sequences that allow for implanted or host cells to remodel and migrate through an otherwise impenetrable matrix (Lutolf et al., 2003; Raeber et al., 2005). Most of these approaches incorporated a peptide that is preferentially sensitive to MMP-2 (Turk et al., 2001; Seliktar et al., 2004; Hanjaya-Putra et al., 2011); however, our findings here suggest that synthetic polymer gels containing peptide cross-links that are more specifically sensitive to MT1-MMP may be better suited to support BMSC-mediated vessel morphogenesis.

Acknowledgments

We are grateful to Dr. Mina J. Bissell, Dr. Hidetoshi Mori, Dr. Joni Mott, and Dr. Cyrus Ghajar for providing us with the ΔCAT-MT1-MMP construct; Dr. Stephen J. Weiss, Dr. Farideh Sabeh, and Dr. Xiao-Yan Li for providing us with the Full-MT1-MMP construct and siRNA against MT1-MMP; Dr. Thomas Lanigan and the University of Michigan Vector Core for providing us with a GFP vector and technical assistance; Dr. Yen Kong for providing insightful discussions; and Dr. Jan Stegemann and Dr. Michael Mayer for providing us with access to their instrumentation. This work was supported by a grant from the National Institutes of Health (R01 HL085339).

Literature Cited

Au P, Tam J, Fukumura D, Jain RK. 2008. Bone marrow-derived mesenchymal stem cells facilitate engineering of long-lasting functional vasculature. Blood 111:4551–4558.
Brooks PC, Stromblad S, Sanders LC, von Schalscha TL, Aimes RT, Stetler-Stevenson WG, Quigley JP, Cheresh DA. 1996. Localization of matrix metalloproteinase MMP-2 to the surface of invasive cells by interaction with integrin alpha v beta 3. Cell 85:683–693.
Caplan AI. 2008. All MSCs are pericytes? Cell Stem Cell 3:229–230.
Carmeliet P, Jain RK. 2000. Angiogenesis in cancer and other diseases. Nature 407:249–257.
Clark RA. 2001. Fibrin and wound healing. Ann NY Acad Sci 936:355–367.
Crisan M, Yap S, Casteilla L, Chen CW, Corselli M, Park TS, Andriolo G, Sun B, Zheng B, Zhang L, Norotte C, Teng PN, Traas J, Schugar R, Deasy BM, Badylak S, Buhring HJ, Giacobino JP, Lazzari L, Huard J, Peault B. 2008. A perivascular origin for mesenchymal stem cells in multiple human organs. Cell Stem Cell 3:301–313.
Egeblad M, Werb Z. 2002. New functions for the matrix metalloproteinases in cancer progression. Nat Rev Cancer 2:161–174.
Farrell DH, al-Mondhiry HA. 1997. Human fibroblast adhesion to fibrinogen. Biochemistry 36:1123–1128.
Ferrari G, Cusella-De Angelis G, Coletta M, Paolucci E, Stornaiuolo A, Cossu G, Mavilio F. 1998. Muscle regeneration by bone marrow-derived myogenic progenitors. Science 279:1528–1530.
Filippov S, Koenig GC, Chun TH, Hotary KB, Ota I, Bugge TH, Roberts JD, Fay WP, Birkedal-Hansen H, Holmbeck K, Sabeh F, Allen ED, Weiss SJ. 2005. MT1-matrix metalloproteinase directs arterial wall invasion and neointima formation by vascular smooth muscle cells. J Exp Med 202:663–671.
Fuchs S, Baffour R, Zhou YF, Shou M, Pierre A, Tio FO, Weissman NJ, Leon MB, Epstein SE, Kornowski R. 2001. Transendocardial delivery of autologous bone marrow enhances collateral perfusion and regional function in pigs with chronic experimental myocardial ischemia. J Am Coll Cardiol 37:1726–1732.

Ghajar CM, Blevins KS, Hughes CC, George SC, Putnam AJ. 2006. Mesenchymal stem cells enhance angiogenesis in mechanically viable prevascularized tissues via early matrix metalloproteinase upregulation. Tissue Eng 12:2875–2888.
Ghajar CM, Chen X, Harris JW, Suresh V, Hughes CC, Jeon NL, Putnam AJ, George SC. 2008a. The effect of matrix density on the regulation of 3-D capillary morphogenesis. Biophys J 94:1930–1941.
Ghajar CM, George SC, Putnam AJ. 2008b. Matrix metalloproteinase control of capillary morphogenesis. Crit Rev Eukaryot Gene Expr 3:251–278.
Ghajar CM, Kachgal S, Kniazeva E, Mori H, Costes SV, George SC, Putnam AJ. 2010. Mesenchymal cells stimulate capillary morphogenesis via distinct proteolytic mechanisms. Exp Cell Res 316:813–825.
Gocheva V, Chen X, Peters C, Reinheckel T, Joyce JA. 2010a. Deletion of cathepsin H perturbs angiogenic switching, vascularization and growth of tumors in a mouse model of pancreatic islet cell cancer. Biol Chem 391:937–945.
Gocheva V, Wang HW, Gadea BB, Shree T, Hunter KE, Garfall AL, Berman T, Joyce JA. 2010b. IL-4 induces cathepsin protease activity in tumor-associated macrophages to promote cancer growth and invasion. Genes Dev 24:241–255.
Grigoriadis AE, Heersche JN, Aubin JE. 1988. Differentiation of muscle, fat, cartilage, and bone from progenitor cells present in a bone-derived clonal cell population: Effect of dexamethasone. J Cell Biol 106:2139–2151.
Hanemaaijer R, Koolwijk P, le Clercq L, de Vree WJ, van Hinsbergh VW. 1993. Regulation of matrix metalloproteinase expression in human vein and microvascular endothelial cells. Effects of tumour necrosis factor alpha, interleukin 1 and phorbol ester. Biochem J 296:803–809.
Hanjaya-Putra D, Bose V, Shen YI, Yee J, Khetan S, Fox-Talbot K, Steenbergen C, Burdick JA, Gerecht S. 2011. Controlled activation of morphogenesis to generate a functional human microvasculature in a synthetic matrix. Blood 118:804–815.
Hauner H, Schmid P, Pfeiffer EF. 1987. Glucocorticoids and insulin promote the differentiation of human adipocyte precursor cells into fat cells. J Clin Endocrinol Metab 64:832–835.
Heissig B, Hattori K, Friedrich M, Rafii S, Werb Z. 2003. Angiogenesis: Vascular remodeling of the extracellular matrix involves metalloproteinases. Curr Opin Hematol 10:136–141.
Hellstrom M, Gerhardt H, Kalen M, Li X, Eriksson U, Wolburg H, Betsholtz C. 2001. Lack of pericytes leads to endothelial hyperplasia and abnormal vascular morphogenesis. J Cell Biol 153:543–553.
Hildenbrand R, Dilger I, Horlin A, Stutte HJ. 1995. Urokinase and macrophages in tumour angiogenesis. Br J Cancer 72:818–823.
Hotary KB, Yana I, Sabeh F, Li XY, Holmbeck K, Birkedal-Hansen H, Allen ED, Hiraoka N, Weiss SJ. 2002. Matrix metalloproteinases (MMPs) regulate fibrin-invasive activity via MT1-MMP-dependent and -independent processes. J Exp Med 195:295–308.
Kachgal S, Putnam AJ. 2011. Mesenchymal stem cells from adipose and bone marrow promote angiogenesis via distinct cytokine and protease expression mechanisms. Angiogenesis 14:47–59.
Kroon ME, Koolwijk P, van Goor H, Weidle UH, Collen A, van der Pluijm G, van Hinsbergh VW. 1999. Role and localization of urokinase receptor in the formation of new microvascular structures in fibrin matrices. Am J Pathol 154:1731–1742.
Lehti K, Allen E, Birkedal-Hansen H, Holmbeck K, Miyake Y, Chun TH, Weiss SJ. 2005. An MT1-MMP-PDGF receptor-beta axis regulates mural cell investment of the microvasculature. Genes Dev 19:979–991.
Lu C, Li XY, Hu Y, Rowe RG, Weiss SJ. 2010. MT1-MMP controls human mesenchymal stem cell trafficking and differentiation. Blood 115:221–229.
Lutolf MP, Lauer-Fields JL, Schmoekel HG, Metters AT, Weber FE, Fields GB, Hubbell JA. 2003. Synthetic matrix metalloproteinase-sensitive hydrogels for the conduction of tissue regeneration: Engineering cell-invasion characteristics. Proc Natl Acad Sci USA 100:5413–5418.
Moon JJ, Saik JE, Poche RA, Leslie-Barbick JE, Lee SH, Smith AA, Dickinson ME, West JL. 2010. Biomimetic hydrogels with pro-angiogenic properties. Biomaterials 31:3840–3847.
Mori H, Gjorevski N, Inman JL, Bissell MJ, Nelson CM. 2009. Self-organization of engineered epithelial tubules by differential cellular motility. Proc Natl Acad Sci USA 106:14890–14895.
Morikawa S, Baluk P, Kaidoh T, Haskell A, Jain RK, McDonald DM. 2002. Abnormalities in pericytes on blood vessels and endothelial sprouts in tumors. Am J Pathol 160:985–1000.
Nakatsu MN, Hughes CC. 2008. An optimized three-dimensional in vitro model for the analysis of angiogenesis. Methods Enzymol 443:65–82.
Ozawa CR, Banfi A, Glazer NL, Thurston G, Springer ML, Kraft PE, McDonald DM, Blau HM. 2004. Microenvironmental VEGF concentration, not total dose, determines a threshold between normal and aberrant angiogenesis. J Clin Invest 113:516–527.
Phelps EA, Landazuri N, Thule PM, Taylor WR, Garcia AJ. 2010. Bioartificial matrices for therapeutic vascularization. Proc Natl Acad Sci USA 107:3323–3328.
Raeber GP, Lutolf MP, Hubbell JA. 2005. Molecularly engineered PEG hydrogels: A novel model system for proteolytically mediated cell migration. Biophys J 89:1374–1388.
Rehman J, Traktuev D, Li J, Merfeld-Clauss S, Temm-Grove CJ, Bovenkerk JE, Pell CL, Johnstone BH, Considine RV, March KL. 2004. Secretion of angiogenic and antiapoptotic factors by human adipose stromal cells. Circulation 109:1292–1298.
Sato H, Takino T, Okada Y, Cao J, Shinagawa A, Yamamoto E, Seiki M. 1994. A matrix metalloproteinase expressed on the surface of invasive tumour cells. Nature 370:61–65.
Seliktar D, Zisch AH, Lutolf MP, Wrana JL, Hubbell JA. 2004. MMP-2 sensitive, VEGF-bearing bioactive hydrogels for promotion of vascular healing. J Biomed Mater Res A 68:704–716.
Siedentop KH, Harris DM, Sanchez B. 1985. Autologous fibrin tissue adhesive. Laryngoscope 95:1074–1076.
Sounni NE, Dehne K, van Kempen L, Egeblad M, Affara NI, Cuevas I, Wiesen J, Junankar S, Korets L, Lee J, Shen J, Morrison CJ, Overall CM, Krane SM, Werb Z, Boudreau N, Coussens LM. 2010. Stromal regulation of vessel stability by MMP14 and TGFbeta. Dis Model Mech 3:317–332.
Toth M, Chvyrkova I, Bernardo MM, Hernandez-Barrantes S, Fridman R. 2003. Pro-MMP-9 activation by the MT1-MMP/MMP-2 axis and MMP-3: Role of TIMP-2 and plasma membranes. Biochem Biophys Res Commun 308:386–395.
Turk BE, Huang LL, Piro ET, Cantley LC. 2001. Determination of protease cleavage site motifs using mixture-based oriented peptide libraries. Nat Biotechnol 19:661–667.
Uttamchandani M, Wang J, Li J, Hu M, Sun H, Chen KY, Liu K, Yao SQ. 2007. Inhibitor fingerprinting of matrix metalloproteases using a combinatorial peptide hydroxamate library. J Am Chem Soc 129:7848–7858.
van Hinsbergh VW, Collen A, Koolwijk P. 2001. Role of fibrin matrix in angiogenesis. Ann NY Acad Sci 936:426–437.
Webster I, West PJ. 2002. Adhesives for Medical Applications. In: Dumitriu S, editor. Polymeric Biomaterials. 2 ed. New York: Marcel Dekker, Inc. pp 703–738.
Yana I, Sagara H, Takaki S, Takatsu K, Nakamura K, Nakao K, Katsuki M, Taniguchi S, Aoki T, Sato H, Weiss SJ, Seiki M. 2007. Crosstalk between neovessels and mural cells directs the site-specific expression of MT1-MMP to endothelial tip cells. J Cell Sci 120:1607–1614.
Yu Q, Stamenkovic I. 1999. Localization of matrix metalloproteinase 9 to the cell surface provides a mechanism for CD44-mediated tumor invasion. Genes Dev 13:35–48.
Zandonella C. 2003. Tissue engineering: The beat goes on. Nature 421:884–886.